UNIVERSITÄT AUGSBURG
Universitätsbibliothek

OPEN ACCESS
OPUS AUGSBURG

# Spectroscopic trace of the Lifshitz transition and multivalley activation in thermoelectric SnSe under high pressure

**Tobias Biesner, Weiwu Li, Alexander A. Tsirlin, Seulki Roh, Pai-Chun Wei, Ece Uykur, Martin Dressel**

**Angaben zur Veröffentlichung / Publication details:**

Biesner, Tobias, Weiwu Li, Alexander A. Tsirlin, Seulki Roh, Pai-Chun Wei, Ece Uykur, and Martin Dressel. 2021. "Spectroscopic trace of the Lifshitz transition and multivalley activation in thermoelectric SnSe under high pressure." *NPG Asia Materials* 13 (1): 12. https://doi.org/10.1038/s41427-021-00283-2.

**Nutzungsbedingungen / Terms of use:**

**CC BY 4.0**

*Dieses Dokument wird unter folgenden Bedingungen zur Verfügung gestellt: / This document is made available under these conditions:*
***CC-BY 4.0: Creative Commons: Namensnennung***
*Weitere Informationen finden Sie unter: / For more information see:*
*https://creativecommons.org/licenses/by/4.0/deed.de*

Biesner et al. *NPG Asia Materials* (2021)13:12
https://doi.org/10.1038/s41427-021-00283-2

NPG Asia Materials

ARTICLE Open Access

# Spectroscopic trace of the Lifshitz transition and multivalley activation in thermoelectric SnSe under high pressure

Tobias Biesner[1], Weiwu Li[1], Alexander A. Tsirlin[2], Seulki Roh[1], Pai-Chun Wei[3,4], Ece Uykur[1] and Martin Dressel[1]

**Abstract**

Multivalley systems offer not only exciting physical phenomena but also the possibility of broad utilization. Identifying an important platform and understanding its physics are paramount tasks to improve their capability for application. Here, we investigate a promising candidate, the semiconductor SnSe, by optical spectroscopy and density functional theory calculations. Upon applying pressure to lightly doped SnSe, we directly monitored the phase transition from semiconductor to semimetal. In addition, heavily doped SnSe exhibited a successive Lifshitz transition, activating multivalley physics. Our comprehensive study provides insight into the effects of pressure and doping on this system, leading to promising routes to tune the material properties for advanced device applications, including thermoelectrics and valleytronics.

## Introduction

Multivalley electronic systems confining charge carriers to a specific momentum have emerged as a key aspect of new technologies[1,2]. These systems have a unique band structure that consists of multiple valence band maxima and conduction band minima with different momenta near the Fermi energy level, providing specific optoelectronic properties[3]. The distinguished momentum dependence in such systems provides an additional degree of freedom for information processing, opening an avenue for valleytronics[4,5]. On the other hand, the multivalley effect improves the efficiency of thermoelectric materials[6,7]. In particular, the Seebeck coefficient can be tuned by increasing the band degeneracy number and the effective mass with an increasing number of valleys[8–10]. In addition to identifying accessible multivalley systems, it is highly desirable to develop proper ways to tune them.

The semiconductor SnSe is a promising multivalley system and is known for its outstanding thermoelectric properties[11–15]. In SnSe, the strong electronic anisotropy with multiple valence band maxima and conduction band minima induces two distinct gaps along the $\Gamma - Y$ and $\Gamma - Z$ directions of the Brillouin zone, corresponding to the zigzag and armchair anisotropy, respectively (see Fig. 1a for the crystal structure)[3,11,16–21]. To further promote multivalley physics, chemical doping was performed to push the Fermi level deep into the valence band, activating multiple hole pockets (Fig. 1b)[6,16,19,21–23]. Furthermore, samples were unintentionally self-doped by Sn vacancies or $SnSe_2$ microdomains, resulting in a small shift in the Fermi level that caused the resistivity of heavily doped SnSe to deviate from its semiconducting behavior, generating a metallic temperature dependence, as depicted in Fig. 1c[17,24].

Pressure is a clean tuning parameter for manipulating material properties[25]. In heavily doped SnSe, a pressure-induced Lifshitz transition occurs, i.e., a change in the Fermi surface topology without a structural transition[26]. At

Correspondence: Tobias Biesner (tobias.biesner@pi1.physik.uni-stuttgart.de) or Weiwu Li (lww60253496@sina.com) or Pai-Chun Wei (pcwei68@ntu.edu.tw)
[1]1. Physikalisches Institut, Universität Stuttgart, Stuttgart, Germany
[2]Experimental Physics VI, Center for Electronic Correlations and Magnetism, University of Augsburg, Augsburg, Germany
Full list of author information is available at the end of the article

© The Author(s) 2021
**Open Access** This article is licensed under a Creative Commons Attribution 4.0 International License, which permits use, sharing, adaptation, distribution and reproduction in any medium or format, as long as you give appropriate credit to the original author(s) and the source, provide a link to the Creative Commons license, and indicate if changes were made. The images or other third party material in this article are included in the article's Creative Commons license, unless indicated otherwise in a credit line to the material. If material is not included in the article's Creative Commons license and your intended use is not permitted by statutory regulation or exceeds the permitted use, you will need to obtain permission directly from the copyright holder. To view a copy of this license, visit http://creativecommons.org/licenses/by/4.0/.

Content courtesy of Springer Nature, terms of use apply. Rights reserved

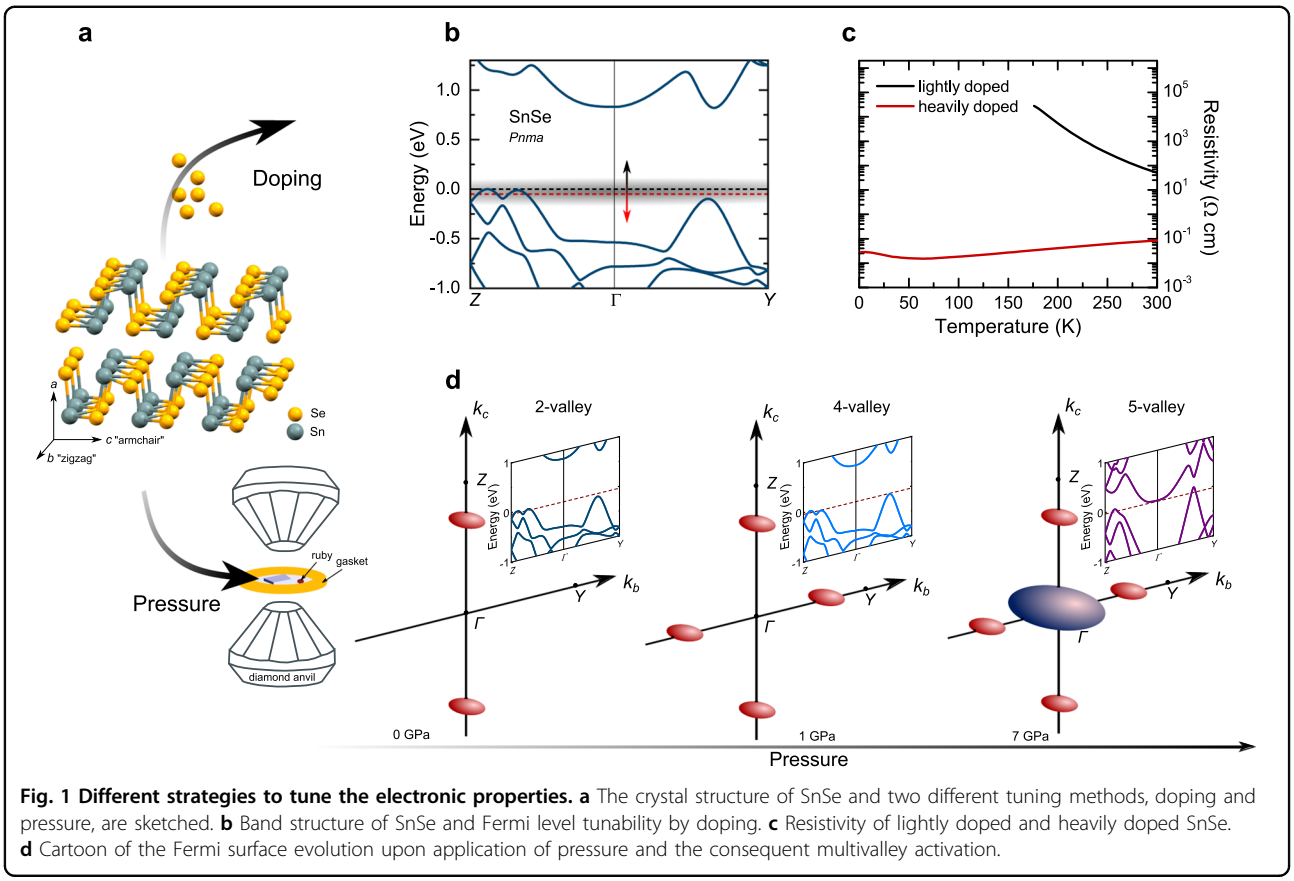


**Fig. 1 Different strategies to tune the electronic properties. a** The crystal structure of SnSe and two different tuning methods, doping and pressure, are sketched. **b** Band structure of SnSe and Fermi level tunability by doping. **c** Resistivity of lightly doped and heavily doped SnSe. **d** Cartoon of the Fermi surface evolution upon application of pressure and the consequent multivalley activation.

0.86 GPa, the compound transforms from a two-valley system to a four-valley system, accompanied by improved thermoelectric properties, providing proof that pressure is a powerful tool to tune the electronic multivalley[27,28]. Density-functional theory (DFT) calculations and transport studies have reported enhanced thermoelectric properties of SnSe upon application of external pressure[29–32]. Although transport measurements[33,34] and theoretical approaches[35,36] provide evidence for a semiconductor-semimetal transition, direct investigations of the electronic structure and its pressure dependence are still lacking. In fact, transport measurements are confined to a cumulative probe of the conduction bands without spectroscopic resolution.

In this study, we employ pressure-dependent infrared spectroscopy to directly map the multivalley electronic band structure of SnSe over a wide pressure range up to 12 GPa in lightly doped and heavily doped samples. By combining these experiments with first-principles calculations, we explain the electronic structure evolution of SnSe from semiconductor-to-semimetal under pressure. In addition to the results from transport studies, in heavily doped SnSe, we observe a Lifshitz transition in the high-pressure range above 7 GPa, where a new electron pocket emerges (see the sketched Fermi surface in Fig. 1d). Our study provides a comprehensive insight into SnSe under pressure, suggesting strategies to tune the optoelectronic and thermoelectric properties to allow device applications in more efficient ways.

## Materials and methods

### Sample preparation and resistivity measurements

Two <100> -cleaved SnSe samples (S1 and S2) with different carrier concentrations (lightly doped and heavily doped) were prepared by the Bridgman method[24]. The carrier concentrations (resistivity) of sample S1 and sample S2 were measured by the Quantum Design® Physical Properties Measurement System (PPMS) to be $3 \times 10^{15}\,\mathrm{cm}^{-3}$ (50.5 Ω cm) and $5 \times 10^{17}\,\mathrm{cm}^{-3}$ (0.086 Ω cm) at 300 K, respectively. With decreasing temperature, sample S1 showed semiconducting-like behavior, whereas sample S2 showed metallic-like behavior. The size of the two samples used for the pressure-dependent optical measurements was approximately 180 (length) × 160 (width) × 40 µm (thickness). Further information about the sample homogeneity can be found in the supplemental material (Fig. S1)

### Optical measurements under high pressure

A screw-driven diamond anvil cell (Almax easyLab) with Type IIa diamonds and an 800 µm culet was used.

Content courtesy of Springer Nature, terms of use apply. Rights reserved

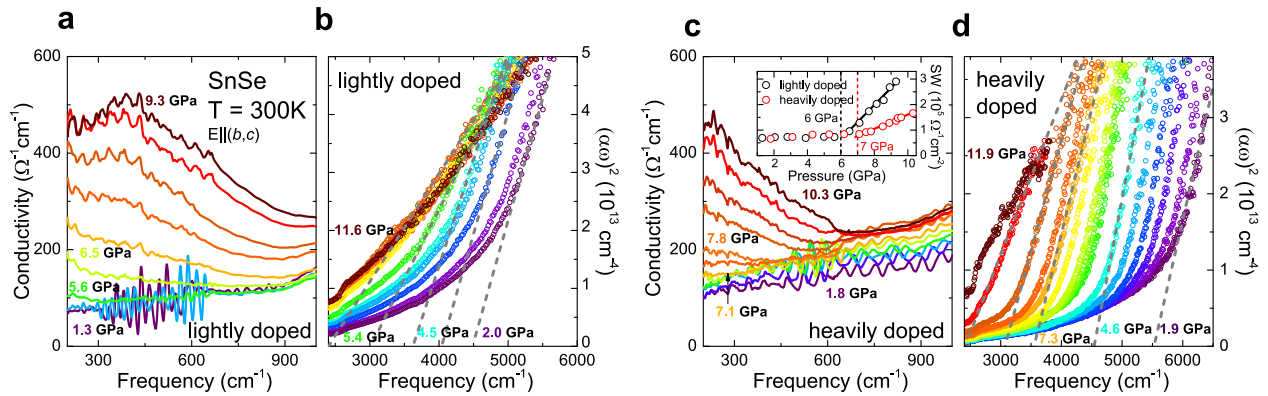


**Fig. 2 Results of the pressure-dependent optical measurements. a**, **c** show far-infrared optical conductivity spectra under several selected pressures for the lightly doped and heavily doped SnSe, respectively. Fabry–Perot oscillations from the samples are visible below the onset of absorbance. The spike lines at the two lowest pressures in **a** might originate from a small void inside the diamond anvil cell that closes under pressure. Inset: spectral weight, SW, of the optical conductivity for both samples as a function of pressure. The black and red dashed lines denote the onset of phase transitions. **b**, **d** show Tauc plots of the optical absorption coefficient $\alpha$ for lightly doped and heavily doped SnSe, respectively. The gray lines indicate estimated energies of the direct optical gap, $E_{g,opt}$, for representative pressures.

CuBe gaskets with a thickness of 60 µm and a hole size of ~250 µm were prepared for sample space, leaving enough free area for multiple ruby spheres, which were used for pressure calibration[37,38] (cf. Fig. S2). CsI was utilized as a quasi-hydrostatic pressure transmitting medium. Reflectance and transmittance spectra were measured by employing a Fourier transform spectrometer (Bruker Vertex 80 v) under near-normal incidence, $E||(b,c)$ at $T =$ 300 K. For the reflectance measurements, we used the CuBe gasket as a reference and corrected the final spectra by the reflectance of CuBe. The transmittance was measured by referencing the transparent pressure media inside the diamond anvil cell. The optical conductivity was determined by modified Kramers–Kronig analysis of the reflectance, as described in the supplemental material. From the data in the mid-infrared range, we calculated the optical absorption coefficient as follows: $\alpha = \frac{1}{d}\ln\left\{\frac{(1-R)^2}{Tr}\right\}$[39], where $R$ and $Tr$ are the reflectance and transmittance, respectively, and $d$ is the sample thickness. Direct optical interband transitions, $E_{g,opt}$, were determined using the Tauc method[40] by extrapolating the linear regime of $(\alpha\omega)^2$. The spectral weight, SW, was determined by integrating the optical conductivity, $\sigma_1(\omega)$, over the frequency, $SW = \int_{\omega_{min}}^{\omega_{max}} \sigma_1(\omega)\, d\omega$, and was directly related to the carrier density and effective mass (see the supplemental material for further information)[40–42]. Extended data sets and further details of the experimental analysis can be found in Figs. S3–S8.

### DFT calculations

Relativistic density-functional band structure calculations were performed in the Wien2K code[43] with the modified Becke-Johnson (mBJ) exchange–correlation functional[44] parametrized according to Ref. [45]. This approach delivers an accurate bandgap for SnSe at ambient pressure and correctly reproduces the pressure of the semiconductor-to-metal transition. In contrast, standard DFT functionals, such as the widely used Perdew-Burke-Ernzerhof exchange–correlation potential[46], tend to underestimate the ambient pressure bandgap and, consequently, the critical pressure where SnSe becomes metallic. Atomic positions from Ref. [47] were used. The band structure and density of states were computed on a well-converged $k$ mesh with 1728 points in the irreducible part of the first Brillouin zone.

## Results

### Optical spectra under pressure

The optical conductivity of the lightly doped SnSe in the far-infrared range upon application of pressure is displayed in Fig. 2a. At ambient pressure, SnSe exhibits a phononic feature at low frequencies, which is also visible in our low-pressure spectra (see Fig. S9). At low pressures, we observe an insulating characteristic without pronounced free charge carriers, i.e., no Drude response[40,42]. With increasing pressure, the low-frequency optical conductivity is increasing with the development of a Drude mode when the pressure exceeds 6 GPa. In addition, the interband contribution changes with increasing pressure, as displayed in Fig. 2b. In particular, the direct optical gap is suppressed continuously, resulting in a redshift. However, at all pressures up to the highest pressure available (11.6 GPa), the gap does not close completely, indicating that the metallization of SnSe above 6 GPa is caused by a band shift across the Fermi level rather than a collapse of the optical gap owing to high pressure. The heavily doped sample (cf. Fig. 2c, d) yields similar results; however, in this

Content courtesy of Springer Nature, terms of use apply. Rights reserved

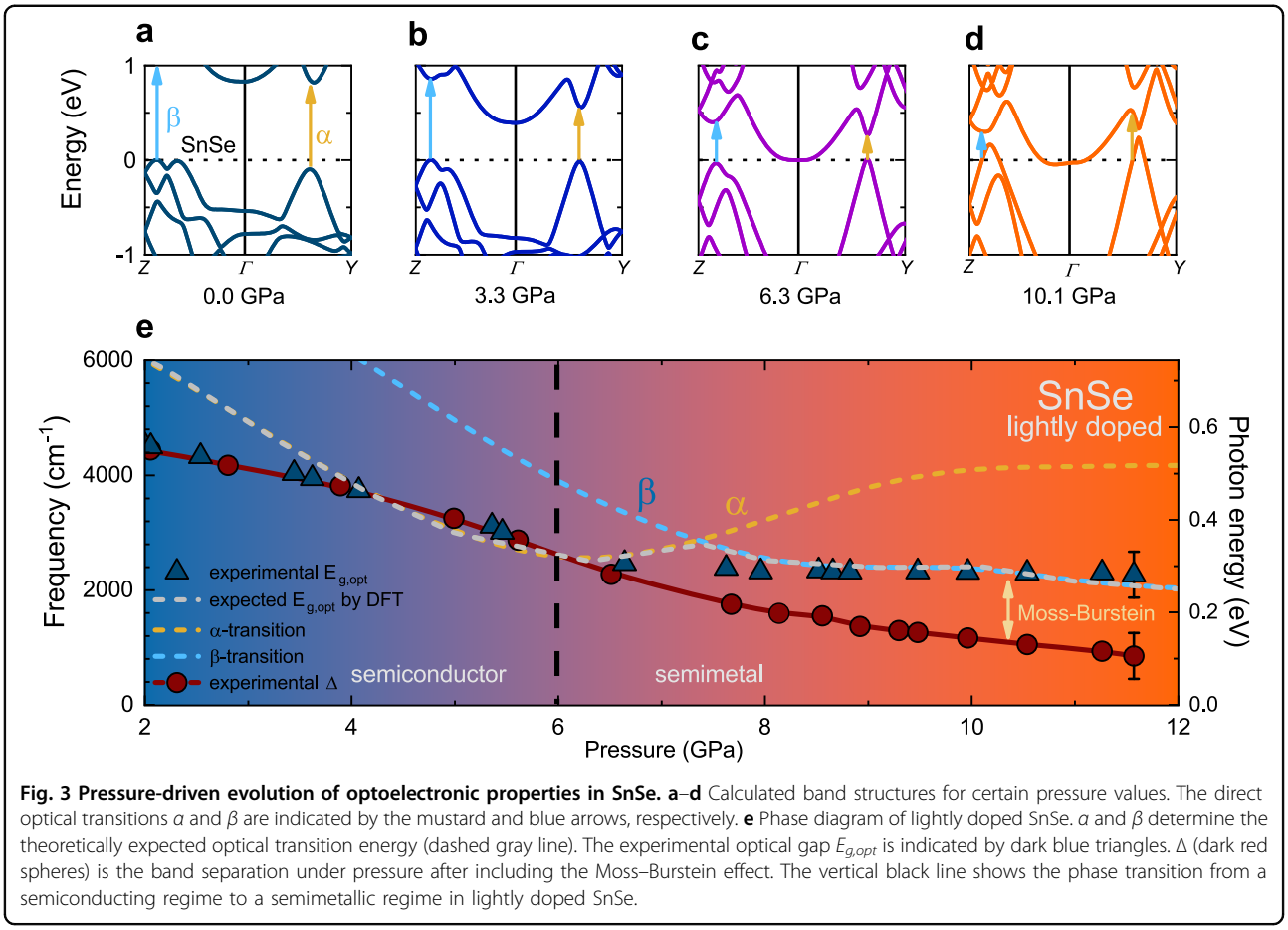


**Fig. 3 Pressure-driven evolution of optoelectronic properties in SnSe. a–d** Calculated band structures for certain pressure values. The direct optical transitions *α* and *β* are indicated by the mustard and blue arrows, respectively. **e** Phase diagram of lightly doped SnSe. *α* and *β* determine the theoretically expected optical transition energy (dashed gray line). The experimental optical gap $E_{g,opt}$ is indicated by dark blue triangles. Δ (dark red spheres) is the band separation under pressure after including the Moss–Burstein effect. The vertical black line shows the phase transition from a semiconducting regime to a semimetallic regime in lightly doped SnSe.

case, a delayed transition above 7 GPa is observed. This delay is most visible in the SW of the low-frequency range (inset of Fig. 2c), where the SW increases more strongly at an earlier pressure for the lightly doped SnSe.

### Optoelectronic properties under pressure

To further scrutinize the electronic evolution under pressure, we compare the experimental results with the results of DFT calculations (Fig. 3a–d). The results along the $Z$–$\Gamma$–$Y$ path of the Brillouin zone are shown for selected pressures. In accordance with the ARPES measurements[17] and previous calculations[31,36], we identify multiple valence band maxima in the $\Gamma-Z$ and $\Gamma-Y$ directions and a minimum of the conduction band at the Γ point, characteristic of the multivalley electronic structure of SnSe. In Fig. 3a, two distinct direct interband transitions, $\alpha$ and $\beta$, are most pronounced. In this case, the transition with lower energy determines the experimental optical gap, $E_{g,opt}$. Thus, at ambient pressure, in the semiconducting phase, $E_{g,opt}$ is governed by transitions along the $\Gamma-Y$ path, $\alpha$.

As the pressure increases, the valence and conduction bands approach the Fermi energy level, $E_F$ (Fig. 3b), and eventually reach $E_F$ at 6.3 GPa (Fig. 3c), rendering a semimetallic picture of the high-pressure phase. Furthermore, above 7 GPa, the optical transition energy $\beta$ becomes smaller than $\alpha$ (see Fig. 3d) and determines the value of $E_{g,opt}$. As the valence band penetrates through $E_F$, the interband transition differs from the band separation, Δ; the Moss–Burstein effect[48,49], $\Delta E_g^{BM}$, occurs. The band separation, Δ, can thus be estimated from the experimental value of $E_{g,opt}$ by correcting for $\Delta E_g^{BM}$, $\Delta = E_{g,opt} - \Delta E_g^{BM}$.

In Fig. 3e, we summarize the results of the DFT calculations ($\alpha$ and $\beta$) and determine the theoretically expected optical gap. From Fig. 2b, we extract the experimentally observed transition energy. To obtain the experimental band separation, we correct the optical gap for the Moss–Burstein effect by using the SW of the low-frequency optical conductivity shown in Fig. 2a (see the supplemental materials for additional information). Here, we see good agreement between the experimental $E_{g,opt}$ value of lightly doped SnSe and the theoretically predicted $E_{g,opt}$ value (for comparison of the band separation, Δ, see the supplemental materials, Fig. S10). This demonstrates that the lightly doped sample captures the genuine electronic structure of SnSe.

Content courtesy of Springer Nature, terms of use apply. Rights reserved

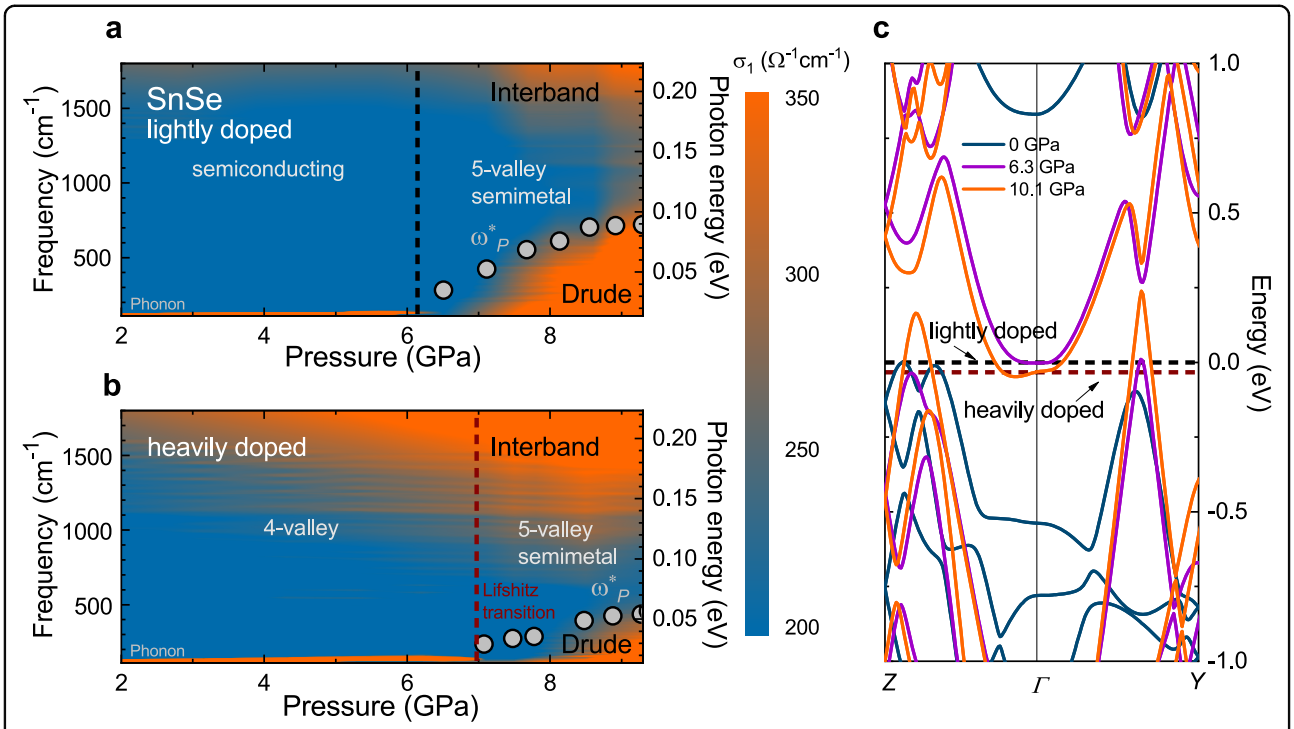


**Fig. 4 Comparison of lightly doped and heavily doped SnSe. a**, **b** Color maps of the optical conductivity, $\sigma_1(\omega)$, as a function of pressure. The screened $\omega_P$ of Drude is plotted as gray dots. The semiconducting-to-semimetallic transition is denoted by a dashed black line for lightly doped SnSe. For heavily doped SnSe, the high-pressure Lifshitz transition is indicated by a dashed red line. **c** Band structure for selected pressure points. The positions of the Fermi level for lightly doped and heavily doped SnSe are indicated by dashed black and red lines, respectively. For heavily doped SnSe, a small shift activates a two-valley state at ambient pressure.

### Effect of self-doping under pressure

The differences between lightly doped and heavily doped SnSe are assumed to originate from a small shift of the Fermi level toward the valence band[17,24]. This shift results in qualitatively and quantitatively different features under pressure as well as distinct resistivity at ambient pressure (see Fig. 1c for the resistivity). In the contour plots in Fig. 4a, b, we compare the evolution of the low-frequency electronic structure of both samples under pressure. At low pressure, the optical conductivity possesses a phonon mode at 120 $cm^{-1}$, which disappears as the Drude response becomes dominant, converting the system into a semimetallic phase (above 6 GPa). Increasing the pressure strengthens the Drude mode as the number of charge carriers increases owing to Fermi surface expansion. At the same time, narrowed interband transitions smear into the low-frequency spectra, increasing their contributions.

Heavily doped SnSe shows a weaker and delayed Drude response (above 7 GPa), as indicated by the SW (Fig. 2c) and the plasma frequencies, $\omega_P$, obtained by a Drude-Lorentz fit (see the supplemental materials). These observations confirm that the Fermi level shifts toward lower energy, explaining the wider optical gap in the heavily doped sample that causes a larger Moss–Burstein contribution, $\Delta E_g^{BM}$. Furthermore, we note that above 10 GPa, the band structure changes only slightly until 14 GPa (Fig. S11 and Fig. S12). In fact, a shift in the Fermi level for heavily doped samples activates the valence band maximum in the $\Gamma-Z$ direction at ambient pressure, as shown in Fig. 4c, causing metallic-like resistivity behavior (Fig. 1c). However, we note that the resistivity of the heavily doped sample is still relatively high, whereas the contribution to the optical conductivity is barely observable ($\sigma_0 \approx 12\,\Omega^{-1}\,cm^{-1}$). The $\Gamma-Y$ direction is further involved at lower pressures, generating an additional hole pocket. This low-pressure transition is suggested by our DFT calculations, in accordance with previously mentioned transport studies, suggesting a Lifshitz transition at 0.86 GPa[27] from a two-valley system to a four-valley system. We note that in the present study, the low-energy limitations of high-pressure optical measurements mask the appearance of the low-pressure Lifshitz transition, whose carrier density is expected to be too small to be detected in our experiment. Importantly, a shift in the Fermi energy causes the conduction band minimum at the Γ point to touch $E_F$ at higher pressures (above 7 GPa) in heavily doped SnSe, creating an additional electron pocket, which is well pronounced in our experimental spectra. This electron pocket further changes the topology of the

Content courtesy of Springer Nature, terms of use apply. Rights reserved

Fermi surface; that is, a Lifshitz transition occurs. Thus, heavily doped SnSe undergoes successive Lifshitz transitions below 1 GPa and above 7 GPa, as shown in Fig. 1d.

Pressure-induced metallization of SnSe is observed by transport measurements, but the transition pressure is different[33,34]. This discrepancy may be caused by variations in the definition of the semiconductor-semimetal transition pressure and differences between powder and single-crystalline samples[33]. Furthermore, we demonstrated that self-doping effects strongly influence the pressure evolution.

## Discussion

For both samples, the semimetallic high-pressure phase originates from a change in the atomic coordinate $z$ of the Sn atom along the $c$ axis. Although the sample remains in the *Pnma* space group[31,34,47], the $c$ axis shows more drastic compression than the other axes[47]. In particular, within the scope of the calculations, only adjusting the lattice parameter does not lead to a metallic phase, even up to 10 GPa. Therefore, we suggest that the previously reported decrease in the Sn $z$-parameter[47] is a crucial factor driving the system into a metallic phase. As previously mentioned[36], pressure affects the SnSe bonds along the $c$ axis, leading to hybridization of Sn-5$s$, Sn-5$p$, and Se-4$p$ orbitals, thus opening an additional conduction channel. In this system, for heavily doped SnSe, the $c$-direction (armchair) is conductive, followed by the $b$-direction (zigzag), ultimately inducing a metallic intralayer state.

The shift in the Fermi level of heavily doped samples, however, crucially changes the pressure dependence. In fact, the successive Lifshitz-type transitions in heavily doped SnSe are distinct from semiconductor-semimetal transitions and the mere creation of a Fermi surface in the lightly doped samples. Owing to the lowered Fermi level, the creation of the electron pocket at the Γ point takes place at a higher pressure, expanding the already existing Fermi surface of hole pockets in heavily doped SnSe.

The multivalley physics induced by the application of pressure could also play a role in thermoelectric devices since the effective mass is affected by the number of activated valleys in a material[8]. The high thermoelectric properties reported in Ref. [27] prove the effects of the multivalley SnSe. However, as the thermoelectric efficiency is determined by a combination of several competing parameters, the effects of an additional electron pocket on the thermoelectric properties remain to be clarified in other studies.

The modified contributions of the $\alpha$- and $\beta$ transitions to the optical gap further offer unique tunability and accessibility to the valley degree of freedom. In particular, with the application of pressure, we can tune the system from a dichroic crystal to a non-dichroic crystal (when $\alpha$ and $\beta$ become comparable). Such a property opens a promising route to valleytronics[1–3].

In summary, we probed the electronic multivalley band structure of SnSe over a broad pressure range by optical spectroscopy. By combining our spectroscopic investigation with DFT calculations, we clarified the semiconductor-semimetal transition in lightly doped SnSe and observed successive Lifshitz transitions in heavily doped samples. We emphasized that self-doping has a considerable influence on the optical properties of SnSe by shifting the Fermi level, which is more pronounced under applied pressure. Our spectroscopic analysis traced the electronic structure evolution under pressure and allowed us to suggest possible applications in the fields of optoelectronics and thermoelectrics by demonstrating versatile tunability under pressure.

#### Acknowledgements
We thank Artem Pronin for the fruitful discussion and Gabriele Untereiner for continuous experimental support.

#### Author details
[1]1. Physikalisches Institut, Universität Stuttgart, Stuttgart, Germany. [2]Experimental Physics VI, Center for Electronic Correlations and Magnetism, University of Augsburg, Augsburg, Germany. [3]Computer, Electrical, and Mathematical Sciences and Engineering Division, King Abdullah University of Science and Technology (KAUST), Thuwal, Saudi Arabia. [4]Center for Condensed Matter Sciences and Center of Atomic Initiatives For New Materials, National Taiwan University, Taipei, Taiwan

#### Funding
The project was supported by the Deutsche Forschungsgemeinschaft (DFG) through grant DR228/52-1. E.U. acknowledges the European Social Fund and the Baden-Württemberg Stiftung for the financial support of this research project by the Eliteprogramm. Open Access funding enabled and organized by Projekt DEAL.

#### Conflict of interest
The authors declare that they have no conflict of interest.

#### Publisher's note
Springer Nature remains neutral with regard to jurisdictional claims in published maps and institutional affiliations.

**Supplementary information** The online version contains supplementary material available at https://doi.org/10.1038/s41427-021-00283-2.

Received: 30 April 2020 Revised: 23 November 2020 Accepted: 14 December 2020
Published online: 05 February 2021

#### References
1. Schaibley, J. R. et al. Valleytronics in 2D materials. *Nat. Rev. Mater.* **1**, 16055 (2016).
2. Behnia, K. Polarized light boosts valleytronics. *Nat. Nanotechnol.* **7**, 488–489 (2012).
3. Lin, S. et al. Accessing valley degree of freedom in bulk Tin (II) sulfide at room temperature. *Nat. Commun.* **9**, 1455 (2018).
4. Rycerz, A., Tworzydlo, J. & Beenakker, C. W. J. Valley filter and valley valve in graphene. *Nat. Phys.* **3**, 172–175 (2007).
5. Li, H.-K. et al. Valley optomechanics in a monolayer semiconductor. *Nat. Photon.* **13**, 397–401 (2019).

Content courtesy of Springer Nature, terms of use apply. Rights reserved

6. Zhao, L.-D. et al. Ultrahigh power factor and thermoelectric performance in hole-doped single-crystal SnSe. *Science* **351**, 141–144 (2016).
7. Zhang, J. et al. Discovery of high-performance low-cost n-type Mg3Sb2-based thermoelectric materials with multi-valley conduction bands. *Nat. Commun.* **8**, 13901 (2017).
8. Snyder, G. J. & Toberer, E. S. Complex thermoelectric materials. *Nat. Mater.* **7**, 105–114 (2008).
9. Pei, Y., Wang, H. & Snyder, G. J. Band engineering of thermoelectric materials. *Adv. Mater.* **24**, 6125–6135 (2012).
10. Xin, J. et al. Valleytronics in thermoelectric materials. *npj Quant. Mater.* **3**, 9 (2018).
11. Zhao, L.-D. et al. Ultralow thermal conductivity and high thermoelectric figure of merit in SnSe crystals. *Nature* **508**, 373–377 (2014).
12. Li, C. W. et al. Orbitally driven giant phonon anharmonicity in SnSe. *Nat. Phys* **11**, 1063–1069 (2015).
13. Liu, F. et al. Phonon anharmonicity in single-crystalline SnSe. *Phys. Rev. B* **98**, 224309 (2018).
14. Skelton, J. M. et al. Anharmonicity in the high-temperature Cmcm phase of SnSe: soft modes and three-phonon interactions. *Phys. Rev. Lett.* **117**, 075502 (2016).
15. Chang, C., Tan, G., He, J., Kanatzidis, M. G. & Zhao, L.-D. The thermoelectric properties of SnSe continue to surprise: extraordinary electron and phonon transport. *Chem. Mater.* **30**, 7355–7367 (2018).
16. Lu, Q. et al. Unexpected large hole effective masses in SnSe revealed by angle-resolved photoemission spectroscopy. *Phys. Rev. Lett.* **119**, 116401 (2017).
17. Wang, Z. et al. Defects controlled hole doping and multivalley transport in SnSe single crystals. *Nat. Commun.* **9**, 47 (2018).
18. Tayari, V. et al. Quasi-two-dimensional thermoelectricity in SnSe. *Phys. Rev. B* **97**, 045424 (2018).
19. Maeda, M. et al. Unusually large chemical potential shift in a degenerate semiconductor: Angle-resolved photoemission study of SnSe and Na-doped SnSe. *Phys. Rev. B* **97**, 121110(R) (2018).
20. Pletikosić, I. et al. Band structure of the IV-VI black phosphorus analog and thermoelectric SnSe. *Phys. Rev. Lett.* **120**, 156403 (2018).
21. Shi, G. & Kioupakis, E. Anisotropic spin transport and strong visible-light absorbance in few-layer SnSe and GeSe. *Nano Lett.* **15**, 6926–6931 (2015).
22. Singh, N. K. et al. The effect of doping on thermoelectric performance of p-type SnSe: Promising thermoelectric material. *J. Alloy. Compd.* **668**, 152–158 (2016).
23. He, W. et al. High thermoelectric performance in low-cost SnS0.91Se0.09 crystals. *Science* **365**, 1418–1424 (2019).
24. Wei, P.-C. et al. Thermoelectric figure-of-merit of fully dense single-crystalline SnSe. *ACS Omega* **4**, 5442–5450 (2019).
25. Mao, H.-K., Chen, X.-J., Ding, Y., Li, B. & Wang, L. Solids, liquids, and gases under high pressure. *Rev. Mod. Phys.* **90**, 015007 (2018).
26. Lifshitz, I. M. Anomalies of electron characteristics of a metal in the high pressure region. *Sov. Phys. JETP* **11**, 1130–1135 (1960).
27. Nishimura, T. et al. Large enhancement of thermoelectric efficiency due to a pressure-induced lifshitz transition in SnSe. *Phys. Rev. Lett.* **122**, 226601 (2019).
28. Mori, H., Usui, H., Ochi, M. & Kuroki, K. Temperature- and doping-dependent roles of valleys in the thermoelectric performance of SnSe: a first-principles study. *Phys. Rev. B* **96**, 085113 (2017).
29. Zhang, Y., Hao, S., Zhao, L.-D., Wolverton, C. & Zeng, Z. Pressure induced thermoelectric enhancement in SnSe crystals. *J. Mater. Chem. A* **4**, 12073–12079 (2016).
30. Yu, H., Dai, S. & Chen, Y. Enhanced power factor via the control of structural phase transition in SnSe. *Sci. Rep.* **6**, 26193 (2016).
31. Efthimiopoulos, I. et al. Effects of temperature and pressure on the optical and vibrational properties of thermoelectric SnSe. *Phys. Chem. Chem. Phys.* **21**, 8663–8678 (2019).
32. Su, N. et al. Pressure-induced enhancement of thermoelectric power factor in pristine and hole-doped SnSe crystals. *RSC Adv.* **9**, 26831–26837 (2019).
33. Yan, J. et al. Pressure-driven semiconducting-semimetallic transition in SnSe. *Phys. Chem. Chem. Phys.* **18**, 5012–5018 (2016).
34. Chen, X. et al. Topological Dirac line nodes and superconductivity coexist in SnSe at high pressure. *Phys. Rev. B* **96**, 165123 (2017).
35. Ghosh, A. et al. Electrical properties of SnSe under high-pressure. *Comput. Condens. Matter* **9**, 77–81 (2016).
36. Peng, J. et al. Pressure-induced improvement in symmetry and change in electronic properties of SnSe. *J. Mol. Model.* **23**, 319 (2017).
37. Dewaele, A., Torrent, M., Loubeyre, P. & Mezouar, M. Compression curves of transition metals in the Mbar range: experiments and projector augmented-wave calculations. *Phys. Rev. B* **78**, 104102 (2008).
38. Datchi, F. et al. Optical pressure sensors for high-pressure–high-temperature studies in a diamond anvil cell. *High. Press. Res.* **27**, 447–463 (2007).
39. Look, D. C. & Leach, J. H. On the accurate determination of absorption coefficient from reflectance and transmittance measurements: application to Fe-doped GaN. *J. Vac. Sci. Technol. B* **34**, 04J105 (2016).
40. Tanner, D. B. *Optical Effects in Solids* (Cambridge University Press, 2019).
41. Basov, D. N., Averitt, R. D., van der Marel, D., Dressel, M. & Haule, K. Electrodynamics of correlated electron materials. *Rev. Mod. Phys.* **83**, 471–541 (2011).
42. Dressel, M. & Grüner, G. *Electrodynamics of Solids: Optical Properties of Electrons in Matter* (Cambridge University Press, 2002).
43. Blaha, P. et al. *WIEN2k, An Augmented Plane Wave + Local Orbitals Program for Calculating Crystal Properties* (Karlheinz Schwarz, Techn. Universität Wien, Austria), 2018. ISBN 3-9501031-1-2.
44. Tran, F. & Blaha, P. Accurate band gaps of semiconductors and insulators with a semilocal exchange-correlation potential. *Phys. Rev. Lett.* **102**, 226401 (2009).
45. Koller, D., Tran, F. & Blaha, P. Improving the modified Becke-Johnson exchange potential. *Phys. Rev. B* **85**, 155109 (2012).
46. Perdew, J. P., Burke, K. & Ernzerhof, M. Generalized gradient approximation made simple. *Phys. Rev. Lett.* **77**, 3865–3868 (1996).
47. Loa, I., Husband, R. J., Downie, R. A., Popuri, S. R. & Bos, J.-W. G. Structural changes in thermoelectric SnSe at high pressures. *J. Phys. Condens. Matter* **27**, 072202 (2015).
48. Burstein, E. Anomalous optical absorption limit in InSb. *Phys. Rev.* **93**, 632–633 (1954).
49. Moss, T. S. The interpretation of the properties of indium antimonide. *Proc. Phys. Soc. B* **67**, 775–782 (1954).


Content courtesy of Springer Nature, terms of use apply. Rights reserved

# Terms and Conditions

Springer Nature journal content, brought to you courtesy of Springer Nature Customer Service Center GmbH (“Springer Nature”).
Springer Nature supports a reasonable amount of sharing of research papers by authors, subscribers and authorised users (“Users”), for small-scale personal, non-commercial use provided that all copyright, trade and service marks and other proprietary notices are maintained. By accessing, sharing, receiving or otherwise using the Springer Nature journal content you agree to these terms of use (“Terms”). For these purposes, Springer Nature considers academic use (by researchers and students) to be non-commercial.
These Terms are supplementary and will apply in addition to any applicable website terms and conditions, a relevant site licence or a personal subscription. These Terms will prevail over any conflict or ambiguity with regards to the relevant terms, a site licence or a personal subscription (to the extent of the conflict or ambiguity only). For Creative Commons-licensed articles, the terms of the Creative Commons license used will apply.
We collect and use personal data to provide access to the Springer Nature journal content. We may also use these personal data internally within ResearchGate and Springer Nature and as agreed share it, in an anonymised way, for purposes of tracking, analysis and reporting. We will not otherwise disclose your personal data outside the ResearchGate or the Springer Nature group of companies unless we have your permission as detailed in the Privacy Policy.
While Users may use the Springer Nature journal content for small scale, personal non-commercial use, it is important to note that Users may not:

1. use such content for the purpose of providing other users with access on a regular or large scale basis or as a means to circumvent access control;
2. use such content where to do so would be considered a criminal or statutory offence in any jurisdiction, or gives rise to civil liability, or is otherwise unlawful;
3. falsely or misleadingly imply or suggest endorsement, approval , sponsorship, or association unless explicitly agreed to by Springer Nature in writing;
4. use bots or other automated methods to access the content or redirect messages
5. override any security feature or exclusionary protocol; or
6. share the content in order to create substitute for Springer Nature products or services or a systematic database of Springer Nature journal content.

In line with the restriction against commercial use, Springer Nature does not permit the creation of a product or service that creates revenue, royalties, rent or income from our content or its inclusion as part of a paid for service or for other commercial gain. Springer Nature journal content cannot be used for inter-library loans and librarians may not upload Springer Nature journal content on a large scale into their, or any other, institutional repository.
These terms of use are reviewed regularly and may be amended at any time. Springer Nature is not obligated to publish any information or content on this website and may remove it or features or functionality at our sole discretion, at any time with or without notice. Springer Nature may revoke this licence to you at any time and remove access to any copies of the Springer Nature journal content which have been saved.
To the fullest extent permitted by law, Springer Nature makes no warranties, representations or guarantees to Users, either express or implied with respect to the Springer nature journal content and all parties disclaim and waive any implied warranties or warranties imposed by law, including merchantability or fitness for any particular purpose.
Please note that these rights do not automatically extend to content, data or other material published by Springer Nature that may be licensed from third parties.
If you would like to use or distribute our Springer Nature journal content to a wider audience or on a regular basis or in any other manner not expressly permitted by these Terms, please contact Springer Nature at

onlineservice@springernature.com